

Regional correlation of the Earth Gravitational Model 2008 with morphogenetic patterns of the Nepal Himalaya

JAN KALVODA¹, JAROSLAV KLOKOČNÍK², JAN KOSTELECKÝ³

¹ Charles University in Prague, Faculty of Science,
Department of Physical Geography and Geocology

² Astronomical Institute, Academy of Sciences of the Czech Republic,
Ondřejov Observatory

³ Czech Technical University in Prague, Faculty of Civil Engineering,
Department of Advanced Geodesy

Abstract

Results of the correlation of regional features of the Earth Gravitational Model 2008 (EGM 08) with morphogenetic and orographical patterns of the Nepal Himalaya are presented. Strong coincidences between large-scale morphogenetic styles of the Nepal Himalaya and the extension of regions with very high positive values of the radial second derivative of the disturbing gravitational potential $T_{\ddot{z}}$ and the most likely in combination with conspicuous areas of high negative values of $T_{\ddot{z}}$ in their close neighbourhood, have been identified. These variable values of $T_{\ddot{z}}$ display significant gravitational signatures of extensive differences and changes in mass density and/or rock massif and regolith distributions which occurred during very dynamic landform evolution of the Nepal Himalaya in the late Cenozoic.

Key words: Earth Gravitational Model 2008, geodynamics, landform evolution, Nepal Himalaya

1. Introduction

Landforms in the Himalaya and neighbouring regions provide evidence for the nature of very dynamic landscape evolution, including extremely high rates of denudation, sediment transfer and deposition. Gravity data are necessary for a better understanding of the processes driving uplift and erosion in active orogenic belts. Spatial and temporal uplift rates have a direct impact on denudation, sediment transfer and deposition, while mountain growth has an effect on regional climate changes. The resulting landforms are also controlled by passive litho-structural features within an uplifting range.

Measurements of the Earth's shape from its surface were the topic of geosciences up to the first half of the 20th century. It was enabled by more than 200 years of developments in mathematics and physics following Issac Newtown's discovery of the gravity law around the year 1667. The gravity field of the Earth has been measured from the orbits of satellites since 1960. By means of satellite measurements, the gravity field is usually described with the help of spherical functions containing a set of coefficients which are unknowns of inverse processes. Geodynamic interpretation of

the results of a gravity survey, which depend on density of matter around measurement sites, also involves determination and explanation of gravity anomalies. These regional anomalies are mainly produced by changes in density of the Earth's crust and by the variable shape of its surface.

The Himalayan mountain ranges and surrounding regions are traditionally accepted as an excellent natural laboratory for gravimetric experiments and survey. For example, some discrepancies in the geodetic and astronomical measurements of the meridian degree length in India carried out by G. Everest and his colleagues in 1840–1859 were a strong stimulation for the J. H. Pratt and G. B. Airy long-term studies of the gravitational attraction of the Himalaya to the direction of the plumb line in its southern foothills. The last decades of the 20th century have seen a remarkable increase in the capabilities of various geophysical, geodetic and geochronological techniques (comp. Watts, 2001; Bishop, 2007) to provide quantitative constraints on landform evolution. Research into the development of mountain reliefs in the Himalaya and neighbouring regions with evidence of active orogeny aims to gain knowledge of the geodynamically critical zones of the Earth's lithosphere as well as the physical properties of rock massifs (Burbank, 1996; Fielding, 1996; Kalvoda and Goudie, 2007). The geomorphological record of late Cenozoic orogenic processes provides valuable evidence of the development of mountain ranges. Among them the Himalaya corresponding to the geodynamic model of the lithospheric plate tectonics is regarded as the most perfectly developed collision orogene of our planet. Studies of the geological structure and of the landforms of Himalaya with distinctive features of active lithospheric plate tectonics produce important facts about the extreme intensity of geodynamic processes which, especially in the Quaternary, remodelled this mountain range and neighbouring areas to the present-day shape.

The correlation of regional features of the Earth Gravitational Model 2008 (EGM 08) with orographical and morphogenetic patterns of the Nepal Himalaya is presented in this paper. We focused on the regional distribution of the free-air gravity anomalies (Δg) and, especially, on the radial second derivative of the disturbing gravitational potential (T_{zz}) computed from EGM 08. Extension of these parameters is compared with large-scale morphostructural landforms of the Nepal Himalaya. Regional coincidences between selected morphogenetic patterns of the Nepal Himalaya and the extension of Δg and T_{zz} have been identified. These recorded gravitational field signatures give strong evidence that landform evolution during the very dynamic collision orogeny of the Himalaya and under the influence of variable climate-morphogenetic processes in the late Cenozoic is characterized by significant changes in rock mass density and distribution. Recent evolution of landforms is accompanied by continuing rapid changes in rock massif volume and large-scale relief patterns of the Himalaya and surrounding areas.

2. Data and methods

2.1 Earth Gravitational Model 2008

The gravity field of the Earth is represented by a spherical harmonic expansion with harmonic geopotential coefficients (Stokes parameters) to a certain degree and order in a form of the so-called “Earth gravitational model”. The data for such a model comes from satellite observations of various types and from terrestrial gravity anomalies measured by gravimeters. The theoretical background and practical examples of the Earth models can be found, e.g. in Schwintzer et al. (1991) or Lemoine et al. (1998).

The National Geospatial-Intelligence Agency (NGA) of the USA has developed a new Earth Gravitational Model 2008, called EGM 08 (Pavlis et al., 2008a,b), intended to replace the US EGM 96 model (Lemoine et al., 1998) which served as one of standards for the Earth models. The new model is complete to degree n and order m i.e. $(n, m) = 2190$ in the spherical harmonic expansion. It means a half-wavelength resolution in equatorial regions on the ground of about $9\text{ km} \times 9\text{ km}$. This is a substantial improvement as opposed to about $50\text{ km} \times 50\text{ km}$ with the EGM 96 and other recent models based only on CHAMP (CHALLENGING Minisatellite Payload) and/or GRACE (Gravity Recovery And Climate Experiment) data.

Geodetic satellites and special research missions CHAMP, GRACE and GOCE (Gravity field and steady state Ocean Circulation Explorer) are experimental bases for improving the knowledge of the geoid and its surface with respect to accuracy and resolution. In reality, formal resolution is increasing with a latitude φ , and it is $9 \cos \varphi$ (km). The resolution is not homogeneous around the world and it depends on the quality of the local data (Fig. 1, colour appendix). For example, the Antarctic region is based solely on the GRACE data. Therefore, it has much lower resolution and the accuracy can also not be homogeneous (Pavlis et al., 2008b).

EGM 08 is a combined gravitational model. The low-frequency portion of the model comes from spaceborne data (namely from the GRACE A/B mission) and the high-frequency part comes from terrestrial and altimetry data. An important contribution to EGM 08 has been made by the terrestrial $5' \times 5'$ (arcminute) mean free-air anomalies measured on the surface and anomalies derived from satellite altimetry over the oceans, almost worldwide. Their precision is usually a few miligals (Huang et al., 2007; Pavlis et al., 2008a,b) which is also true for the commission error of the gravity anomalies computed from the EGM 08 harmonic coefficients. Exceptions from the high precision are some high mountain and polar regions (Fig. 2, colour appendix), such as the Tibetan Highland and its neighbouring areas and Antarctica. The Shuttle Radar Topography Mission (SRTM), with a resolution of 3×3 arcseconds (1×1 arcsec for USA and Canada), has tremendously improved our knowledge of the topography of about 80% of the Earth’s land surface (Rabus et al., 2003). This improvement in the data, satellite as well as terrestrial, goes together with the refinement of data processing algorithms.

After intensive testing of EGM 08 (e.g. Huang et al., 2007; Pavlis et al., 2008b; Klokočník et al., 2008a,b, 2010) it is accepted that it performs in some cases equally well as (or better than) detailed gravimetric products from ground surveys. It provides a new paradigm for a variety of geoscience applications. The Tibetan part of Asia

belongs among the areas with lower accuracy (Fig. 2, colour appendix), but signal to noise ratio is still large enough to ensure that the derived functions of EGM 08 nearly always show realistic features.

2.2 Functions of the gravitational potential of EGM 08

We made use of generic software for ‘gravitational synthesis’ (Holmes et al., 2006). The program computes (among other quantities) the gravity anomalies and the first and second derivatives of the gravitational potential. The following quantities are actually computed for our applications:

- 1) the free-air gravity anomaly, more precisely “spherically approximated gravity anomaly”, $\Delta g = -\partial T/\partial r - 2T/r$, where T is the disturbing gravitational potential $T = V - U$ with the normal potential U , as represented by the Geodetic Reference System (Moritz, 1984);
- 2) the second derivatives of T on the main diagonal of the Marussi tensor, i.e. T_{xx} , T_{yy} and T_{zz} , namely the second radial derivative $T_{zz} \approx T_{rr} = \partial^2 T / \partial r^2$, where r is the geocentric radius of a general computation point. It should be always outside the sphere of radius R which is a scaling parameter of the EGM 08. All presented results were computed for the height $h = 0$ km (ground level) and $5' \times 5'$ angular grid.

The gravity anomaly Δg is approximately equal to the first radial derivative of the disturbing gravity potential, and the T_{zz} parameter is approximately equal to the first radial derivative (radial gradient) of the gravity anomaly. The gravity anomaly is defined through the fundamental gravimetric equation and in spherical approximation reads as follows

$$\Delta g(r, \theta, \lambda) = - \left(\frac{\partial}{\partial r} + \frac{2}{r} \right) T(r, \theta, \lambda) = \frac{GM}{R^2} \sum_{n=2}^{\max} (n-1) \left(\frac{R}{r} \right)^{n+2} = T_n(\theta, \lambda),$$

where R is the radius of the Earth and $T_n(\theta, \lambda)$ is an approximation of T_n (component of T) by spherical functions, n is the degree of harmonic expansion, (θ, λ) are co-latitude and longitude. We still use Δg , but just the radial gravity perturbations, i.e. the first derivatives of the potential, would be sufficient. The reason is that the comparison of our results from the global gravitation field model with local terrestrial data in the form of Δg is very effective.

The second radial derivative of the disturbing gravitational potential in spherical approximation is

$$T_{rr}(r, \theta, \lambda) = \frac{\partial^2}{\partial r^2} T(r, \theta, \lambda) = \frac{GM}{R^3} \sum_{n=2}^{\max} (n+1)(n+2) \left(\frac{R}{r} \right)^{n+3} = T_n(\theta, \lambda)$$

with

$$T_n(\theta, \lambda) = \sum_{m=0}^n (C_{n,m} \cos m\lambda + S_{n,m} \sin m\lambda) P_{n,m}(\cos \theta),$$

where $C_{n,m}$ and $S_{n,m}$ are harmonic geopotential coefficients (Stokes parameters) from EGM 08 and $P_{n,m}$ are associated Legendre functions. Here for EGM 08 we have $n_{max} = 2190$.

2.3 Morphogenetic interpretation of the extension of the gravitational potential over the Earth's surface

The radial second derivatives of the disturbing gravitational potential T_{zz} are proportional to the mean curvature of the geoid. The value of curvature of the geoid is determined by the actual distribution of the matter, including the configuration of landforms, which is mainly the result of the long-term evolution of the Earth's crust. For these reasons, free-air gravity anomalies and second derivatives of the disturbing gravitational potential give evidence of peculiarities of the present-day Earth's shape and its regional mass distribution as well as the intensity and integration of activities of very variable endogenous and climate-morphogenetic processes. For example, regions of the collision orogeny are characteristic by conspicuous compressions of rock massifs in the near-surface part of the Earth's crust, and, therefore, by positive free-air gravity anomalies. Negative free-air gravity anomalies are indicated in regions of tectonically conditioned discontinuities or sinking of the Earth's surface and in regions with very intensive erosion of rocks and transport of regolith away. On the contrary, long-term activity of climate-morphogenetic processes in tectonically calm regions and in areas of active epeirogenesis resulted in the development of large planation surfaces, which are very close to geophysical planes of the same gravitational potential. On planation surfaces of different genesis and age, smoothed by denudation or accumulation, values of the second derivatives of the disturbing gravitational potential T can be expected in the range of approximately ± 100 Eötvös.

We focused on the radial second derivative of the disturbing gravitational potential T_{zz} that show more details than the gravity anomaly itself. Moreover, T_{zz} is always mathematically more powerful than the other second derivatives T_{xx} , T_{yy} . Two radial derivatives make each (n, m) term of order m squared while the other 2nd derivatives are of order $n \cdot m$ or m . The l squared power of the radial components keeps the T_{zz} sensitivity superior to the higher degree terms and through them to the finer structures of the curvature of the geoid. We computed Δg and T_{zz} for selected regions of the world and we founded graphical database of their values after EGM 08 for various geodynamical interpretations. At the same time, we opened a systematic screening of connections and relations between the radial derivatives of the disturbing gravitational potential T_{zz} with large-scale landform patterns and their morphogenetic features.

The main results of the integrated research in the region of Nepal Himalaya are presented in this paper. We computed the free-air gravity anomaly Δg and the second radial derivative of the disturbing gravitational potential T_{zz} over the region of the Nepal Himalayas as well as over the whole Tibet Highland and neighbouring regions (Figs. 3 and 4, colour appendix) for large-scale morphogenetic correlations with the landform pattern and its palaeogeographical evolution. The second derivatives T_{zz} at ground level actually disclose many more details than the first derivatives of the potential and led to new possibilities of geodynamic interpretations. In all presented figures with presentations of Δg (Figs. 3 and 8, colour appendix) and T_{zz} (Figs. 4, 9, colour appendix and Fig. 16) non-linear scales are used to emphasize the signal and the zero value of the computed quantities is always in green. The units for free-air gravity anomalies (Δg) are

1 mGal (or miligal) = 10^{-5} m s^{-2} , and those for second radial derivatives of the disturbing gravitational potential (T_{zz}) are $1 \text{ E} = 1 \text{ Eötvös} = 10^{-12} \text{ s}^{-2}$.

3. Results

Cartographical demonstration of the extension of free-air gravity anomalies Δg and second radial derivative of the disturbing gravitational potential T_{zz} clearly express the main orographical features of the Tibetan Highland and surrounding areas (Figs. 3 and 4, colour appendix). The Pamir, Kuen Lun, Tibetan Highland, Tarim Basin and Cchaidam Basin as well as the Pamir, Karakoram, Himalayan mountain ranges, Indogangetic Plain and Brahmaputra Lowland are conspicuously expressed. Moreover, specific morphostructural patterns of this part of Asia, e.g. large-scale distribution of ridges, valleys or intermountain basins and an eccentric bending of the river network east of the Himalaya are very remarkable. In the Himalayan mountain ranges (Fig. 5) and the Tibetan Highland positive gravity free-air anomalies Δg computed from EGM 08 expressively predominate (Fig. 3, colour appendix), and negative gravity free-air anomalies Δg are typical for the Indogangetic Plain and Siwalik Hills. On the contrary, large areas with negative values of the radial second derivative of the disturbing potential T_{zz} computed from EGM 08 (Fig. 4, colour appendix) are found especially in central parts of the Himalaya and the Karakoram.

We performed a regional correlation between orographical position and the morphogenetic distribution of values of Δg and T_{zz} in the Nepal Himalaya. Glacial, nival and periglacial landform patterns of the High Himalaya in the central part of Nepal as well as its southern foreland display the features of orogenetic processes (Figs. 6 and 7). High-mountain reliefs of the Nepal Himalaya are manifested by outstanding positive free-air gravity anomalies Δg and mostly positive radial second derivatives of the disturbing gravitational potential T_{zz} computed from EGM 08 (comp. Figs. 8 and 9, colour appendix). The Nepal Himalaya have not yet attained isostatic equilibrium, since the endogenous processes producing their uplift are more active than erosion and denudation. It has recently been recognized that mountain building on this scale is directly related to late Cenozoic climate changes in Asia (e.g. Fielding, 1996; Burbank et al., 2003; Bishop, 2007).

High-mountain landforms and rapid exhumation of deep crystalline rocks in the Nepal Himalaya are the result of morphotectonic processes, as well as denudation and erosional efficiency under different palaeoclimatic conditions during the late Cenozoic. Research on landform patterns of peculiar relief types suggests extremely high rates of denudation, sediment transfer and deposition (Kalvoda, 1992; Burbank et al., 2003; Fort, 2004). Recent climate-driven morphogenetic processes in the extremely dissected relief with an elevational gradient of over 7000 m are very active in the framework of extraglacial, glacial, periglacial and seasonally cold/warm humid and/or semi-arid zones. The geomorphological observations suggest (comp. Burbank et al., 1996, 2003; Kalvoda, 2007; Kalvoda and Goudie, 2007; and others) that the frequency and magnitude of recent landform changes are increasing from a very cold and dry extraglacial zone across a large periglacial area up to a subtropical landscape with

humid climatic conditions. Dynamic changes of landscape pattern are important evidence of the present-day severe natural hazards and risks (e.g. Kalvoda and Rosenfeld, 1998; Bishop, 2007).

Weathered, eroded and transported material is accumulated in the southern Himalayan foreland represented by the Siwalik Hills (Fig. 7) and the Indus, Ganga and Brahmaputra lowlands. The rock base of prevalingly fluvial sediments of the Indogangetic Plain and the Siwalik Hills in Nepal are built up of the folded Pliocene to Middle Pleistocene molasse sediments plunging to the north below the front of Palaeozoic limestone and sandstone formations of the Lesser Himalaya. Described morphostructural accumulation basins with folded sediments of late Cenozoic age in the foreland of the Nepal Himalaya display negative free-air gravity anomalies Δg . In contrast to that, radial second derivatives of the disturbing gravitational potential T_{zz} (comp. Figs. 8 and 9, colour appendix) have in these orographical zones variable values in the range between approximately +100 and -160 E.

In the Nepal Himalaya, it is evident that there is a large range of values of Δg approximately between +660 and -260 mGal (Fig. 8, colour appendix) in comparison with those of the High Himalaya (the Great Himalayan Range) and the Gangetic Plain. It is produced by a very variable present mass distribution in the region of active orogeny, which is a large space of the Cenozoic collision between the Indian and Asian lithospheric plates (Fig. 5). Moreover, rapid landform evolution in the Nepal Himalaya is indicated not only by a large range of values of T_{zz} approximately between +1100 and -700 E (Fig. 9, colour appendix), but also, especially, by its specific configuration and sharp differences in orographical and morphogenetic positions. These phenomena are a consequence and manifestation of the variable integration of extremely active morphotectonic and climate-morphogenetic processes in the late Cenozoic.

The main morphogenetically conspicuous types of the space configuration of values of the radial second derivative of the disturbing gravitational potential T_{zz} have been identified with large-scale regional landform patterns of the Nepal Himalaya. For example, at the foot of the western steep semi-graben slopes, belonging to the Mustang Range, a very conspicuous fault zone runs with the main direction NNE-SSW (Fig. 10). This intermontane basin is represented by expressively negative free-air gravity anomalies Δg as well as negative radial second derivatives of the disturbing gravitational potential T_{zz} computed from EGM 08. It is in a sharp contrast with highly positive values of Δg and T_{zz} on both flanks of the Thakkhola semi-graben basin surrounded by mountain ranges in the north of the High Himalaya. To the south, the bottom of the more than 6000 m deep Kali Gandaki canyon, trending approximately NNE-SSW across the High Himalaya (Fig. 11), is between the Dhaulagiri (8172 m) and Annapurna (8078 m) at 1260 m a.s.l. The extremely deep canyon of the Kali Gandaki valley is indicated by striking negative free-air gravity anomalies Δg and negative radial second derivatives of the disturbing gravitational potential T_{zz} . On the contrary, the Dhaulagiri and Annapurna Massifs display highly positive values of Δg and T_{zz} computed from EGM 08.

In the Mahabharath Lakh mountain range, the Barzami fault zone is a distinctive landform pattern which has been morphotectonically very active in the Quaternary and resulted in the origin of the Pokhara intermontane basin (Fig. 12) in the confluence area

of the Seti Khola and Sarandi Khola rivers. The Pokhara intermontane basin is situated on the south of the Annapurna Massif (8078 m) and Machapucchare (6998 m) and its floor dips from 1200 to 520 m a.s.l. The Quaternary fluvial, lacustrine and slope sediments in the Pokhara intermontane basin are mostly composed of fragments of granites, gneisses, quartzites, low- to medium-grade metamorphic calcareous rocks and limestones. The huge polygenetic accumulations in the Pokhara Basin are products of rapid weathering, erosion and transport processes of rock disintegration of the evolving mountain ranges in the late Cenozoic. Extreme morphostructural differences between the Annapurna Massif and Mahabharath Lakh (Fig. 12) are also displayed by the geographical distribution of free-air gravity anomalies Δg and radial second derivatives of the disturbing gravitational potential T_{zz} computed from EGM 08. Highly positive values of Δg and T_{zz} in the High Himalaya are in striking contrast with their essentially lower values in the Mahabharath Lakh. In the Pokhara intermontane basin and surrounding areas, very negative values of Δg are characteristic while the area of negative values of T_{zz} is conspicuously smaller.

The Chomolongma Massif with Mount Everest (Sagarmatha, 8847 m), Lhotse (8501 m) and Lhotse Shar (8383 m) is situated in the central part of the strongly glaciated regions of the Rongbuk, Karma, Barun, Imja and Khumbu valleys (Fig. 13). It is a region of very high positive free-air gravity anomalies Δg and also positive radial second derivatives of the disturbing gravitational potential T_{zz} . On the contrary, negative values of T_{zz} , which are detected in the south of the Chomolongma Massif, follow the very deep canyon of the Dudh Kosi river in the High Himalaya. Long-term weathering processes of crystalline rocks in extremely cold and semiarid climatic conditions and consecutive rapid and/or slow mass movements are the initial agents of the very effective cascade of glacial, nival, periglacial and river erosion resulting in a larger-scale transport of regolith away from the orogenetically uplifted high-mountain ranges. The presented landform patterns of the High Himalaya (Fig. 14) are manifested by highly positive free-air gravity anomalies Δg . However, values of the radial second derivative of the disturbing gravitational potential T_{zz} proved a more variable structure of its positive (and in some regions also negative) values of T_{zz} which is in harmony with the described extreme regional activity of morphogenetic processes.

The extremely dissected high-mountain relief around the antecedent valley of the Arun river in the East Nepal Himalaya uncovers the biotite gneisses, migmatites, amphibolites and muscovite-biotite schists. The Arun river valley cuts through the High Himalaya mountain ranges between Mount Everest (8847 m) and Kangchendzönga (8593 m) and it is incised down to as deep as 1050 m a.s.l. (Fig. 15). The extremely deep canyon of the Arun river is indicated by striking negative free-air gravity anomalies Δg and negative radial second derivatives of the disturbing gravitational potential T_{zz} computed from EGM 08.

Geomorphological research in the Nepal Himalaya suggests a significant correlation and feedbacks between the rate of tectonic exhumation of deep crystalline rocks and the intensity of climate-morphogenetic processes. The very high rates of glacial and periglacial modelling of mountain massifs, slope movements and erosive incision of canyon-like valleys also stimulate isostatic compensation (Wager, 1937; Seeber and Gornitz, 1983; Watts, 2001; Kalvoda et al., 2004). The effectiveness of weathering and

the transport of its products increases with the frequency of alternations of glacial, periglacial and fluvial processes during the evolution of the high-mountain landscape of the Himalaya.

Regions of the Nepal Himalaya with occurrence of very high positive values of the second radial derivative of the disturbing gravitational potential T_{zz} , and the most likely in combination with areas of high negative values of T_{zz} in their close neighbourhood (Fig. 16), have been identified. These variable values of T_{zz} display significant gravitational signatures of conspicuous differences and changes in mass density and/or rock massif and regolith distributions, which occurred during very dynamic landform evolution and rapid geodynamic events in the late Cenozoic. These Himalayan areas can be accepted as one of the most active morphogenetic regions of the Earth.

4. Conclusions

The extremely high intensity of denudation and transport of weathered and eroded material during the Cenozoic orogeny in the collision zone between the Indian and Asian lithospheric plates correlates with the large-scale morphogenetic style of the Nepal Himalaya and its present-day mass distribution as recorded by the regional extension of values of second radial derivative of the disturbing gravitational potential T_{zz} , computed from the Earth gravitational model EGM 08.

It is suggested that Himalayan regions with the occurrence of conspicuous combinations of significantly high positive or negative values of radial second derivatives of the disturbing gravitational potential T_{zz} are characterized by significantly active geodynamic and geomorphic processes and hazards. Moreover, we suppose that variable large-scale configurations of values of anomalies of radial second derivatives of the disturbing gravitational potential T_{zz} give evidence of the long-term operation of certain complexes of morphogenetic processes producing the evolution of not only distinctive topographic features, but also, especially, of specific relief types of the Earth. This concept is based on knowledge of the effective tuning of paleogeographical changes in the extent, dynamics and integration of the morphotectonic and climate-morphogenetic processes during the evolution of very variable landform patterns of the planet. It can be thoroughly tested during further developments of the gravitational model EGM 08 by comparison of relevant gravimetrical results obtained in morphogenetically variable regions of the Earth.

Acknowledgments

The paper was completed in the framework of the project MSM 0021620831 “Geographical systems and risk processes in the context of global changes” and the project CEDR LC 506 “Recent dynamics of the Earth” of the Ministry of Education of the Czech Republic. The authors are grateful to N. K. Pavlis and other authors of the Earth Gravitation Model 2008 for an invitation to long-term cooperation.

References

- BISHOP, P. (2007): Long-term landscape evolution: linking tectonics and surface processes. *Earth Surface processes and landforms*, 32, 3, p. 329–365.
- BURBANK, D. W., LELAND, J., FIELDING, E., ANDERSON, R. S., BROZOVIC, N., REID, M. R., DUNCAN, C. (1996): Bedrock incision, rock uplift and threshold hillslopes in the northwestern Himalayas. *Nature*, 379, p. 505–510.
- BURBANK, D. W., BHYTHE, A. E., PUTKONEN, J., PRATT-SITLAULA, B., GABET, E., OSKIN, M., BARROS, A., OJHA, T. P. (2003): Decoupling of erosion and precipitation in the Himalayas. *Nature*, 426, p. 652–655.
- FIELDING, E. J. (1996): Tibet uplift and erosion. In: Burg, J. P. (ed.), *Uplift and exhumation of metamorphic rocks, the Himalayan Tibet region*. *Tectonophysics*, 260, (1–3), p. 55–84.
- FORT, M. (2004): Quaternary glaciation in the Nepal Himalaya. In: Ehlers, J. and Gibbard, P. L. (eds.): *Quaternary Glaciation – Extent and Chronology. Part III: South America, Asia, Africa, Australia, Antarctica*. *Development in Quaternary Science*, 2c, p. 261–278.
- HOLMES, S. A. et al. (2006): A Fortran program for very-high-degree harmonic synthesis (Harmonic Synth), version 05/01/2006.
- HUANG, J., KOTSAKIS, C., GRUBER, T. (2007): Review of Evaluation Methods and Test Results for the Quality Assessment of Earth Gravity Models. IUGG XXIV, GS 002: Gravity field, Perugia; IAG/IGFS Joint Working Group, evaluation of the gravity field model PGM 2007A, http://users.auth.gr/~kotsaki/IAG_JWG.
- KALVODA, J. (1992): Geomorphological Record of the Quaternary Orogeny in the Himalaya and the Karakoram. In: *Development in Earth Surface Processes*, 3, Elsevier, 315 p., Amsterdam.
- KALVODA, J. (2007): Dynamics of landform evolution in the Makalu – Barun region, Nepal Himalaya. *Geografický časopis*, 59, 2, p. 85–106, Bratislava.
- KALVODA, J., ROSENFELD, CH., eds. (1998): *Geomorphological Hazards in High Mountain Areas*. The GeoJournal Library, Vol. 46, Kluwer Academic Publishers, 314 p., Dordrecht, Boston, London.
- KALVODA, J., KOŠLER, J., SVOJTKA, M. (2004): Morphotectonic evidence for chronodynamics of uplift in the East Nepal Himalaya. *Acta Universitatis Carolinae, Geographica*, 39, 1, p. 149–162, Prague.
- KALVODA, J., GOUDIE, A. S. (2007): Landform evolution in the Nagar region, Hunza Karakoram. In: Goudie, A. S., Kalvoda, J. (eds.): *Geomorphological variations*. P3K Publishers, 407 p., p. 87–126, Prague.
- KLOKOČNÍK, J., NOVÁK, P., PEŠEK, I., KOSTELECKÝ, J., WAGNER, C. A. (2008a): EGM 08: tests of the model and simulations for GOCE. IAG Symp. on Gravity, Geoid and Earth Observations 2008, Chania, Crete, Greece, 23–27 June, www.geomatlab.tuc.gr/GGEO2008.
- KLOKOČNÍK, J., KOSTELECKÝ, J., WAGNER, C. A. (2008b): Improvement in the radial accuracy of altimeter-satellite orbits to the geopotential. *Earth-Science Reviews*, 91, 1–4, p. 106–120, Amsterdam.
- KLOKOČNÍK, J., KOSTELECKÝ, J., NOVÁK, P., WAGNER, C. A. (2010): Detecting impact craters aided by the detailed global gravitational model EgM 2008. *Acta Geodynamica et Geometrialia*, 7,1 (157), p. 71–97.
- LEMOINE, F. J., KENYON, S. C., FACTOR, J. K., TRIMMER, R. G., PAVLIS, N. K., CHINN, D. S., COX, C. M., KLOSKO, S. M., LUTHCKE, S. B., TORRENCE, M. H., WANG, Z. M., WILLIAMSON, R. G., PAVLIS, E. C., RAPP, R. H., OLSON, T. R. (1998): The Development of the Joint NASA GSFC and the National Imagery and Mapping Agency (NIMA), Geopotential Model EGM 96, NASA/TP-1998-206861.
- MORITZ, H. (1984): Geodetic Reference System 1980. *Bulletin Geodesique*, 58, p. 388–398.
- PAVLIS, N. K., HOLMES, S. A., KENYON, S. C., FACTOR, J. K. (2008a): An Earth Gravitational Model to degree 2160: EGM 2008. Presentation at Session G3: “GRACE Science Applications”, EGU Vienna.
- PAVLIS, N. K., HOLMES, S. A., KENYON, S. C., FACTOR, J. K. (2008b): EGM 2008: An Overview of its Development and Evaluation. Lecture, IAG Symp. GGEO 2008, 23–27 June 2008, Chania, Crete, Greece.
- RABUS, B., EINEDER, M., ROTH, A., BAMLER, R. (2003): The Shuttle radar topography mission – a new class of digital elevation models acquired by spaceborne radar. *Photogrammetry and Remote Sensing*, 57, p. 241–262.

- SCHWINTZER, P., REIGBER, CH., MASSMANN, F. H., BARTH, W., RAIMONDO, J. C., GERSTL, M., LI, H., BIANCALE, R., BALMINO, G., MOYNOT, B., LEMOINE, J. M., MARTY, J. C., BOUDON, Y., BARLIER, F. (1991): A New Earth Gravity Model in Support of ERS-1 and SPOT-2, GRIM4S1/C1, DGFI and GRGS. Report to DARA and CNES, München and Toulouse.
- SEEBER, L., GORNITZ, V. (1983): River profiles along the Himalayan arc as indication of active tectonics. *Tectonophysics*, 92, p. 335–367.
- WAGER, R. L. (1937): The Arun river drainage pattern and the rise of the Himalaya. *Geographical Journal*, 89, p. 239–250.
- WATTS, A. B. (2001): *Isostasy and Flexure of the Lithosphere*. Cambridge University Press, 458 p., Cambridge.

Résumé

Regionální korelace modelu gravitačního pole Země 2008 s morfo-genetickými styly Nepálského Himálaje

V práci jsou předloženy výsledky korelace regionálních rysů modelu gravitačního pole Země 2008 (EGM 08) s morfo-genetickými styly Nepálského Himálaje. Byly zjištěny podstatné shody mezi oblastmi s vysokými kladnými hodnotami radiální složky druhé derivace poruchového gravitačního potenciálu T_{zz} , které jsou často doprovázeny blízkými areály výrazně záporných hodnot T_{zz} , a specifickými morfo-genetickými styly pohoří. Tyto variabilní hodnoty T_{zz} představují významný gravitační záznam značných rozdílů a změn hustoty hmoty resp. rozčlenění horninových masivů a regolithu, které jsou důsledkem velmi dynamického vývoje povrchových tvarů Nepálského Himálaje v mladším kenozoiku.

*Jan Kalvoda
Charles University in Prague
Faculty of Science
Department of Physical Geography and Geoecology
Albertov 6
128 43 Praha 2
Czech Republic
e-mail: kalvoda@natur.cuni.cz*

*Jaroslav Klokočník
Astronomical Institute
Academy of Sciences of the Czech Republic
Ondřejov Observatory
Fričova 298
251 65 Ondřejov,
Czech Republic
e-mail: jklokochn@asu.cas.cz*

*Jan Kostecký
Czech Technical University in Prague
Faculty of Civil Engineering
Department of Advanced Geodesy
Thákurova 7
166 29 Prague 6
Czech Republic
e-mail: kost@fsv.cvut.cz*



Fig. 5 The mountain ranges of southern Asia were thrown up by the collision of the Indian and Asian plates. From right to left are indicated conspicuous morphostructural units: the Tibetan Highland, the Tibetan Himalaya with the Indus and Tsang Po river networks, the High Himalaya (the Great Himalayan Range), the Lesser Himalaya, the Siwalik Hills and the Indogangetic Plain. The Mount Everest (Sagarmatha, 8847 m), Lhotse (8501 m) and Makalu (8475 m) Massifs and the Arun river network in the Nepal Himalaya are situated on the right side of the lower part of this Apollo Mission photography.



Fig. 6 Landform patterns of the High Himalaya in the central part of Nepal display the features of active orogenic processes and the uplift of mountain ranges is more rapid than erosion and denudation. The mountain building is directly related to late Cenozoic climate changes in Asia. (Figures 6 and 7 Jan Kalvoda)



Fig. 7 Recent alluvial fan with deposits ranging from coarse sand to block debris originated during repeated monsoon rains in the Indogangetic Plain at the foot of the Siwalik Hills in Nepal. The Siwalik Hills are built up of the folded Pliocene to Middle Pleistocene mollase sediments originated as products of erosion and denudation in mature morphogenetic stages of the Himalayan orogeny.



Fig. 10 The large semiarid headwater region of the Kali Gandaki and Mustang Chu rivers is situated in the Thakkhola semi-graben. At the foot of the western steep slopes of the Thakkhola semi-graben, belonging to the Mustang Range, a very conspicuous fault zone runs with the main direction NNE–SSW. In the central part of the intermontane basin are sediments of the Pliocene Tetang and the Thakkhola Formations of Quaternary age. (Figures 10–12 Jan Kalvoda)



Fig. 11 The north-eastern part of Dhaulagiri (8172m) and Tukuchetse (6875 m) Massifs in the High Himalaya are situated very close to the Kali Gandaki gorge (1200–2400 m a.s.l.). In the foreground, below slopes of the western cliffs of the Nilgiri (7148 m) in the Annapurna Massif, large accumulations of Upper Pleistocene and Holocene fluvio-glacial, slope and eolian sediments are developed.



Fig. 12 The Pokhara intermontane basin is situated on the south of the Annapurna Massif (8078m) and Machapucchare (6998m) and its floor dips from 1200 to 520 m a.s.l. The huge polygenetic accumulations in the Pokhara Basin are products of rapid weathering, erosion and transport processes of rock disintegration of the evolving mountain ranges in the late Cenozoic.

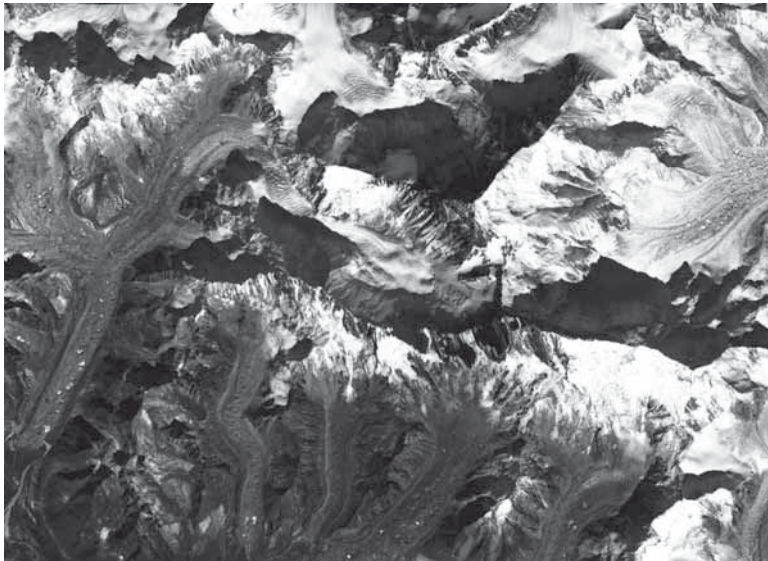


Fig. 13 The Chomolungma Massif with Mount Everest (Sagarmatha, 8847 m), Lhotse (8501 m) and Lhotse Shar (8383 m) is surrounded by the strongly glaciated Rongbuk, Karma, Barun, Imja and Khumbu valleys. It is a region of very high positive free-air gravity anomalies Δg and also positive radial second derivatives of the disturbing gravitational potential T_{zz} . (Satellite photography from Digital Globe Series, May 2003)



Fig. 14 Cryogenic, nival and glacial erosion landforms with conspicuous detachment planes of giant mass movements in the steep walls and rock slopes of Peak IV (6720 m), situated in the Makalu Massif consisting of Miocene leucocratic granites and black gneisses, are an example of the characteristic relief patterns of the High Himalaya. Long-term weathering processes of crystalline rocks in extremely cold and semiarid climatic conditions and consecutive rapid and/or slow mass movements are the initial agents of the very effective erosion in high-mountain ranges. (Figures 14 and 15 Jan Kalvoda)



Fig. 15 The Arun river valley of the antecedent origin cut through the High Himalaya mountain ranges between the Sagarmatha (Mount Everest, 8847 m) and/or Makalu Massifs (8475 m) and the Jannu (7712 m) and/or Kangchendzönga (8593 m) Massifs (in the background on the horizon). On the 110 km long tie-line between the Sagarmatha and Kangchendzönga Massifs, the canyon floor lies at an altitude of 1750 m a.s.l. Moreover, more to the south, at the confluence with the Barun Khola river, the Arun valley is incised into the crystalline rocks of the High Himalaya as deep as 1050 m a.s.l.

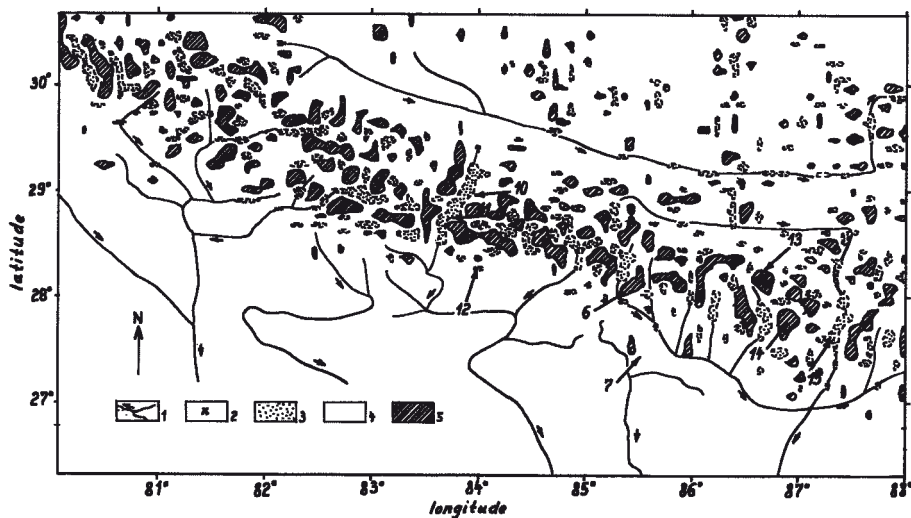


Fig. 16 The main regions of the Nepal Himalaya with significantly high positive or negative values of radial second derivatives of the disturbing gravitational potential T_{zz} (comp. Fig. 9) and the geographical position of landform areas selected as examples of their morphogenetic interpretation. Explanations: 1 – main rivers in the Nepal Himalaya, 2 – mountains rising above 8000 m a.s.l., 3–5 areas with values of radial second derivatives of the disturbing gravitational potential T_{zz} , computed from EGM 08 in the range: 3 – from -700 to -201 E, 4 – from -200 to +200 E, 5 – from +201 to +1100 E. Arrows illustrate geographical positions of representative landform patterns of the Nepal Himalaya which are described in this paper and numbers indicate the regions of photographs presented in figures 6, 7, 10, 11, 12, 13, 14 and 15.

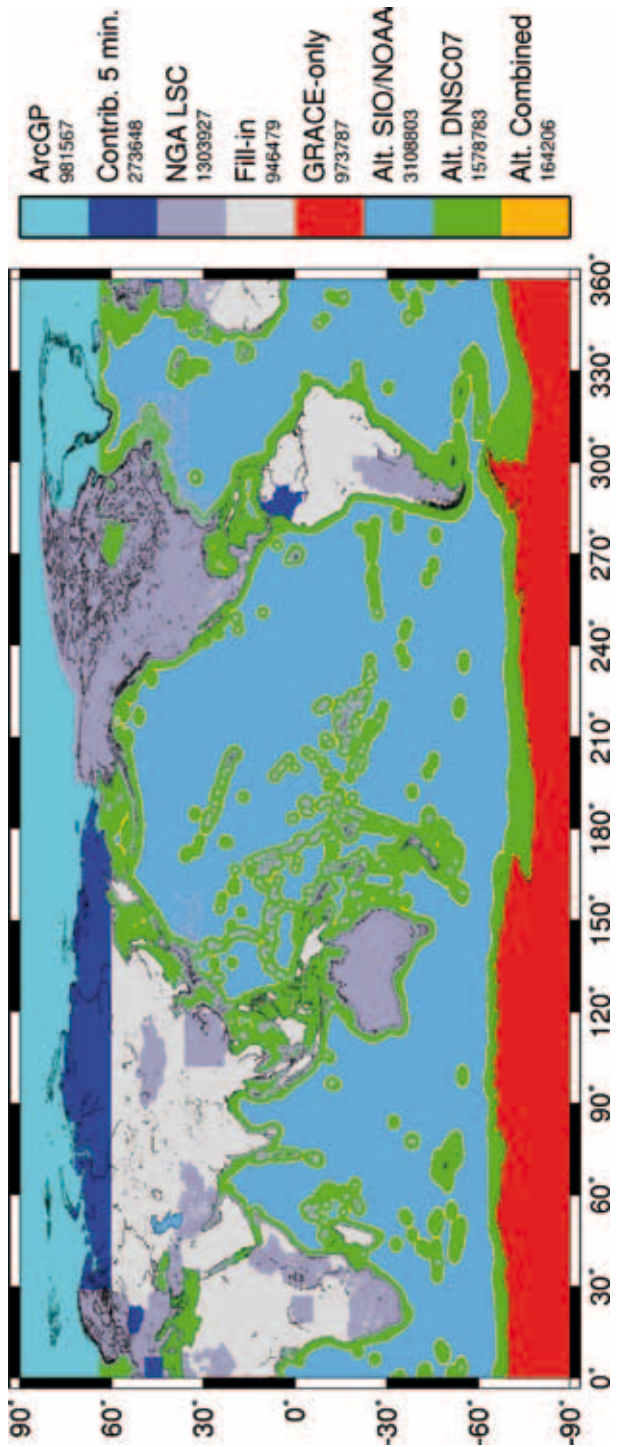


Fig. 1 Data source of gravity anomalies for EGM 08 (Pavlis et al., 2008 a, b, more details by Pavlis, private communication). Explanations:

ArcGP: 5×5 minute mean gravity anomalies which were estimated as part of the Arctic Gravity Project.

Contrib. 5 min: 5×5 minute mean gravity anomalies which were contributed to the project "ready-made". These mean values were estimated by the contributing person or agency.

NGA LSC: 5×5 minute mean gravity anomalies which were estimated using Least Squares Collocation (LSC) by NGA.

Fill-in: 5×5 minute mean gravity anomalies which were computed from the spectral "cut-and-paste" set of coefficients, where, up to $n = 720$ the coefficients represent the (proprietary) 5×5 minute mean gravity anomalies, and from $n = 721$ to $N_{\max} = 2159$ they represent the gravity anomalies implied by the Residual Terrain Model effects.

Alt. SIO/NOAA: 5×5 minute mean gravity anomalies which were estimated by D. Sandwell and W. Smith, using altimetry data.

Alt. DNOSC07: 5×5 minute mean gravity anomalies which were estimated by O. Andersen and P. Knudsen, using altimetry data.

Alt. Comb.: 5×5 minute mean gravity anomalies which were estimated as a linear combination of the SIO/NOAA and DNOSC07 values (to avoid jump discontinuities).

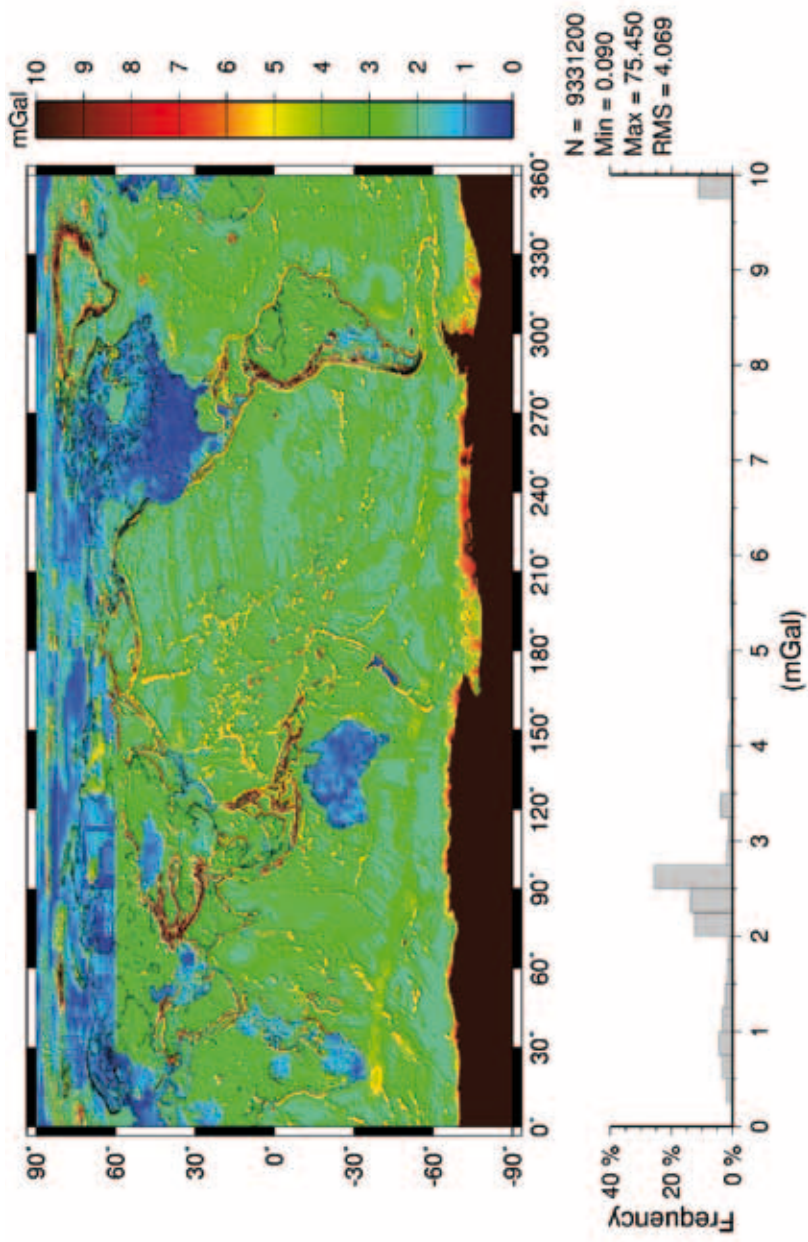


Fig. 2 Precision of gravity anomalies or formal standard deviations (“commission errors”) of the free-air gravity anomalies derived from the harmonic geopotential coefficient errors of EGM 08 till degree and order 2190. The coloured scale is in mGal; 1 milliGal = 10^{-5} m s⁻². This data enabled the rough estimation of signal/noise (S/N) ratios for the gravity anomalies computed over an area of interest. While N for the Himalaya is relatively large (≈ 20 mGal), the signal S itself is also large (between 200–600 mGal), and a typical ratio of S/N ≈ 10 –30 can be expected.

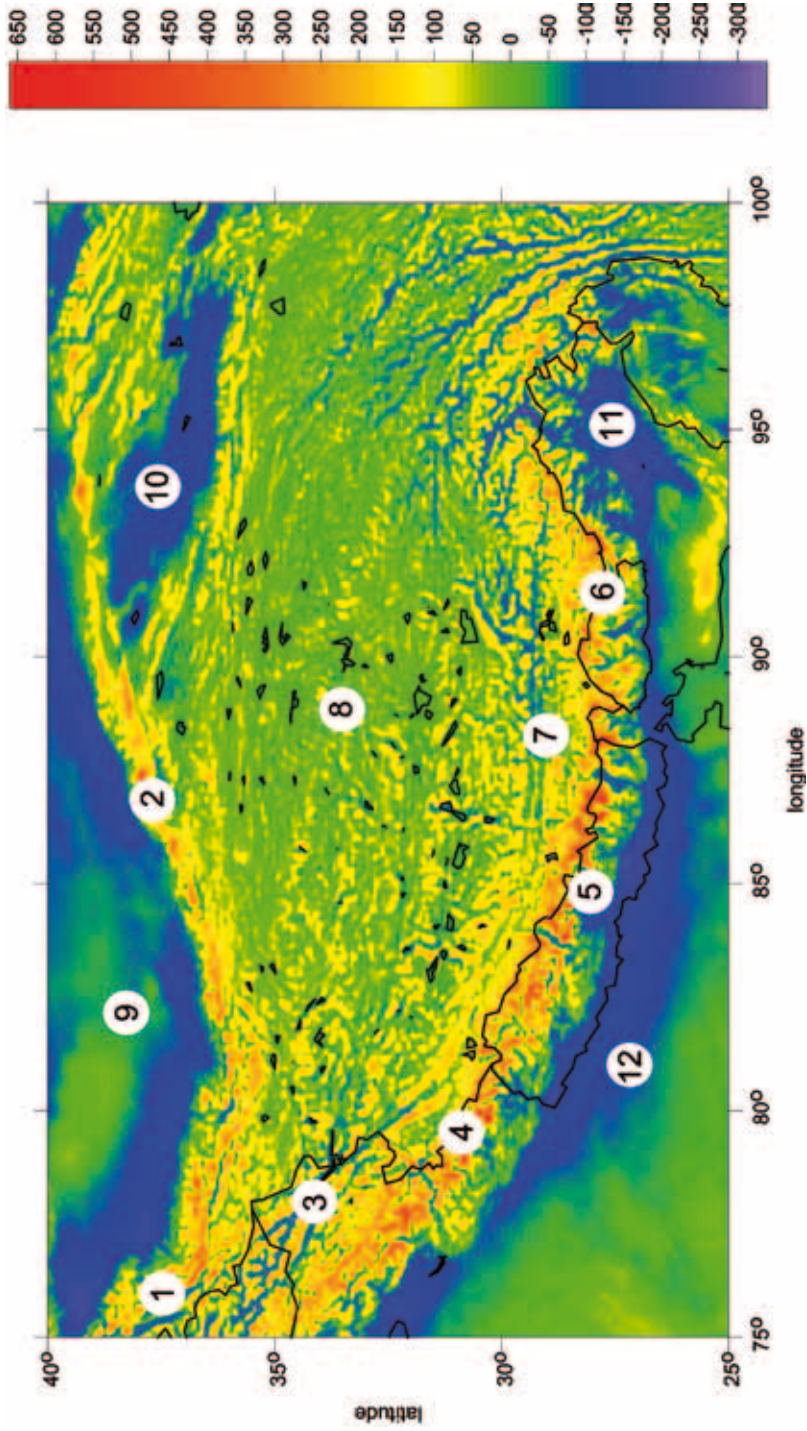


Fig. 3 Free-air gravity anomalies Δg computed from EGM 08 coefficients to 2190 over the Tibetan Highland and surrounding areas. The coloured scale is in mGal. Selected large-scale orographical units: 1 – Pamir, 2 – Kuen Lun, 3 – Karakoram, 4 – western Himalaya, 5 – Central (Nepal) Himalaya, 6 – eastern Himalaya, 7 – Tibetan Himalaya, 8 – Tibetan Highland, 9 – Cchaidam Basin, 10 – Brahmaputra Lowland, 11 – Indogangetic Plain.

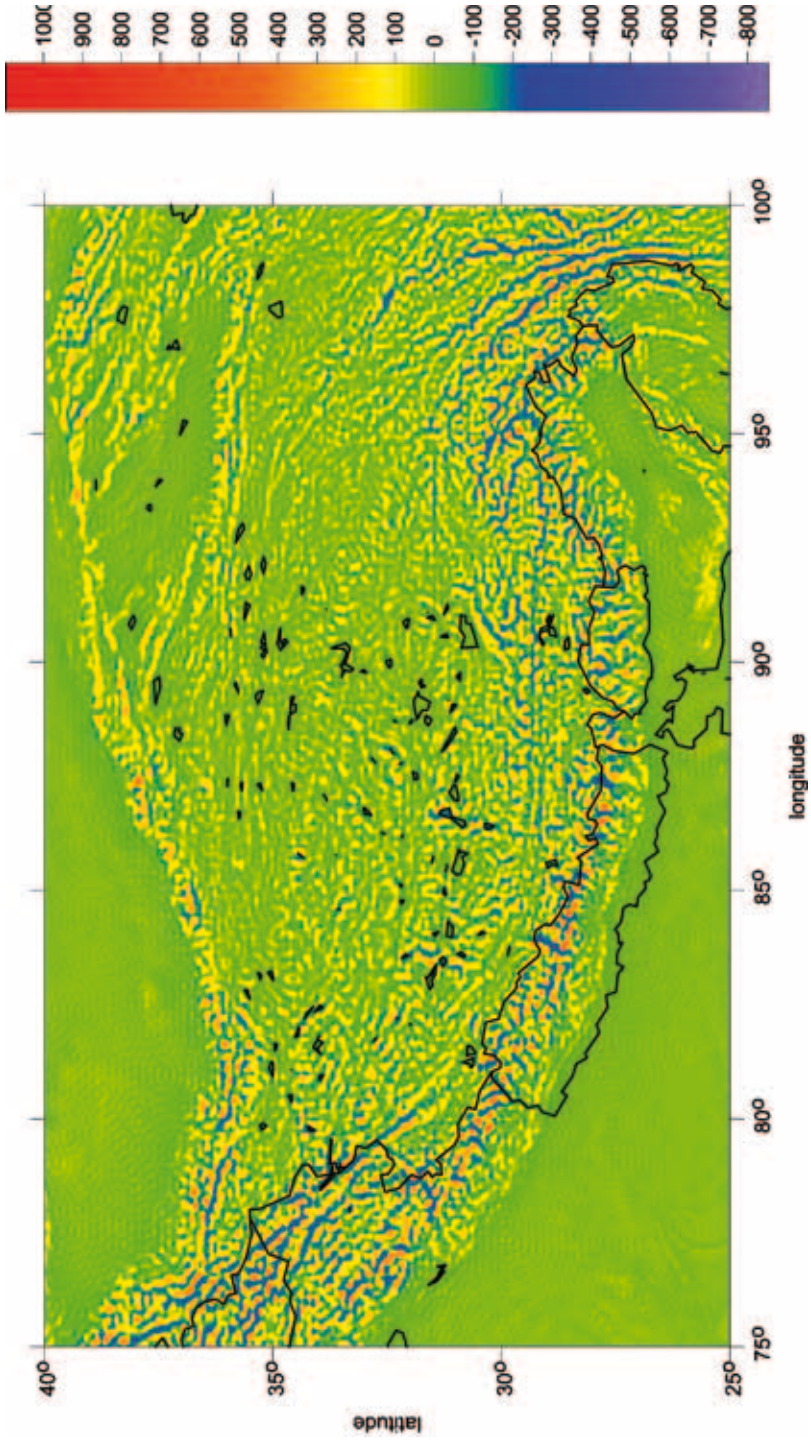


Fig. 4 Radial second derivatives of the disturbing gravitational potential T_z computed from EGM 08 coefficients to 2190 over the Tibetan Highland and neighbouring areas. The coloured scale is in E; $1 \text{ Eötvös} = 10^{-12} \text{ s}^{-2}$. Main large-scale orographical units are indicated in Fig. 3 and the southern part of the region is also shown in Fig. 5.

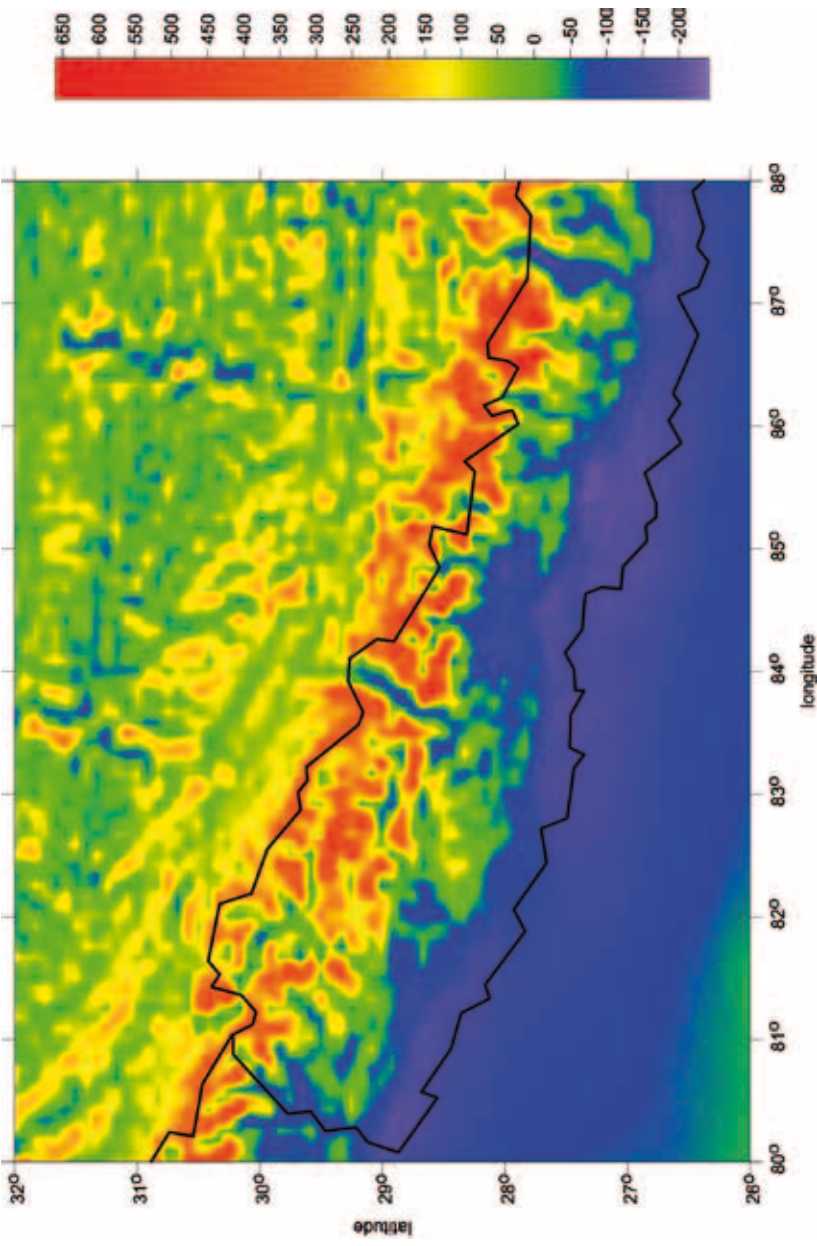


Fig. 8 Free-air gravity anomalies Δg computed from EGM 08 coefficients to 2190 for the Nepal Himalaya and its neighbouring areas in Tibet and the Gangetic Plain. The coloured scale is in mGal. Geologically, a large range of values of Δg approximately between +660 and -260 mGal in comparison of the High Himalaya (the Himalayan Range) and the Gangetic Plain is substantial.

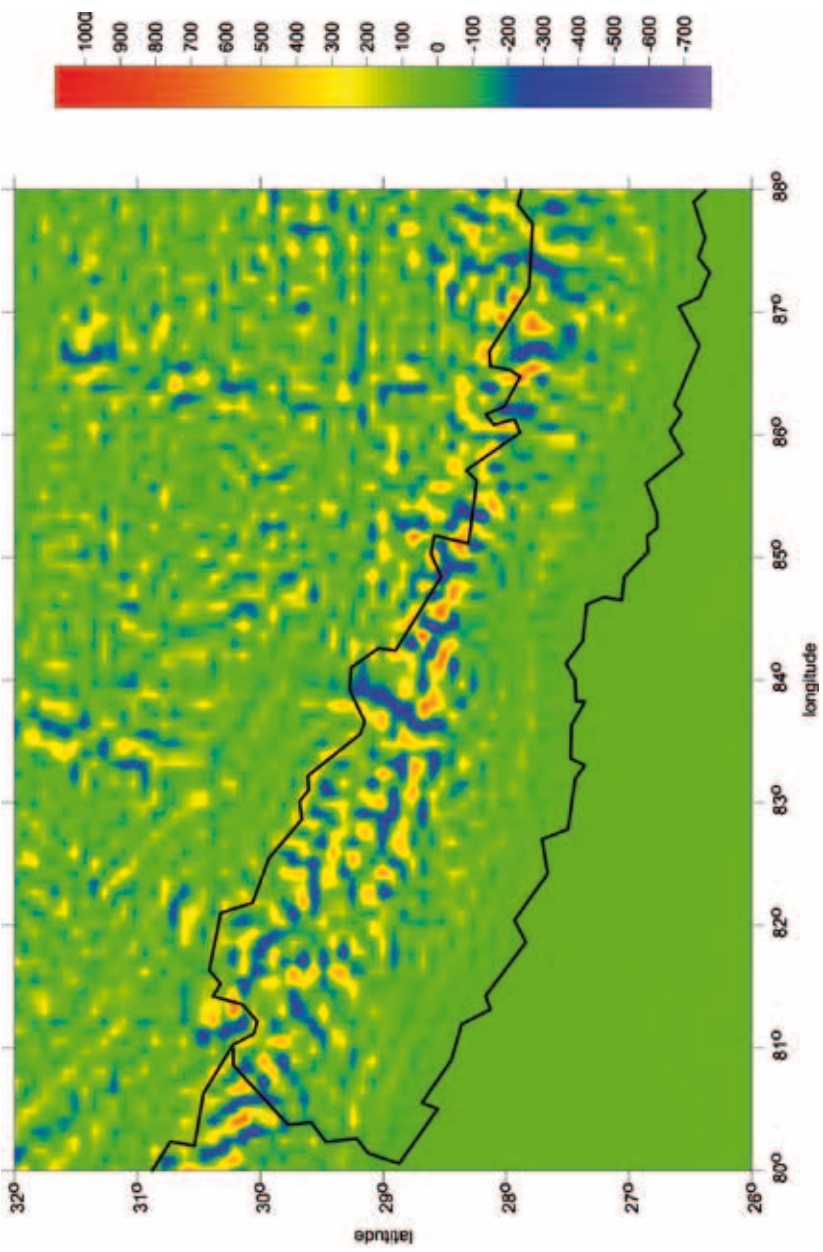


Fig. 9 Radial second derivatives of the disturbing gravitational potential T_{zz} computed from EGM 08 coefficients to 2190 for the Nepal Himalaya and its neighbouring areas in Tibet and the Ganga Plain. The coloured scale is in E. Rapid landforms evolution in the Nepal Himalaya is indicated not only by a large range of values of T_{zz} approximately between +1100 and -760 E, but also, especially, by its very specific configuration and sharp differences in orographical and morphogenetic positions.